The effect of dissolved oxygen and ultrasonic pretreatment on the Cr(VI) removal efficiency with manganese ferrite

Wenjuan Shen[a],*, Zixin Yao[a], Zhan Liu[a], Menghan Xiao[a], JuanJuan Zhang[a], Xu Zhang[b], Fengjiao Quan[a], Jianfen Li[a],*, Wenqing Wang[a], Shunxi Zhang[a], Xing Peng[b],*, Zhenhua Qin[a]

[a]*College of Chemical and Environmental Engineering, Wuhan Polytechnic University, Wuhan 430023, China, emails: wenjuan_shen@whpu.edu.cn (W. Shen), whpulijfen@126.com (J. Li), 2696135644@qq.com (Z. Yao), 1581008791@qq.com (Z. Liu), 1051322647@qq.com (M. Xiao), 1509872142@qq.com (J.J. Zhang), fengjiaoquan@whpu.edu.cn (F. Quan), 359781590@qq.com (W. Wang), 1664894572@qq.com (S. Zhang), whpuchem@126.com (Z. Qin)*
[b]*Key Laboratory of Pesticide and Chemical Biology of Ministry of Education, Institute of Environmental and Applied Chemistry, Central China Normal University, Wuhan 430079, China, emails: pengxing185@163.com (X. Peng), 506539205@qq.com (X. Zhang)*

ABSTRACT

Hexavalent chromium (Cr(VI)) removal from aqueous solution with magnetic manganese ferrite has been demonstrated to be an effective method, however, its wide application is restricted as manganese ferrite was easy to aggregate by magnetism. Meanwhile, the effect of dissolved oxygen on the performance of magnetic manganese ferrite was still unclear. Hence, this study aimed to investigate the influence of ultrasound pretreatment and dissolved oxygen on Cr(VI) removal efficiency with manganese ferrite nanoparticles. The characterization results of pristine manganese ferrite indicated that the prepared nanoparticles were spherical with diameter around 200 nm, and the valence for manganese and iron element were +2 and +3, respectively. Subsequently, we compared the removal percentage of Cr(VI) in the presence or absence of dissolved oxygen with or without ultrasound pretreatment, and the results demonstrated that ultrasound pretreatment and the presence of dissolved oxygen increased the Cr(VI) removal percentage to 100%. Moreover, the high-resolution X-ray photoelectron spectroscopy (HR-XPS) results exhibited that the valence of Mn and Fe element did not changed during the Cr(VI) removal process, suggesting that Cr(VI) was separated from water via adsorption pathway. This deduction could be further verified by the HR-XPS spectra of Cr 2p after the reaction in the Ar and air condition. This research revealed the effect of ultrasound pretreatment and dissolved oxygen on Cr(VI) removal with manganese ferrite and provided fundamental theory for the wide application of magnetic manganese ferrite for water treatment.

Keywords: Manganese ferrite; Cr(VI); Ultrasound; Dissolved oxygen

1. Introduction

Heavy metals pollution in water and soil attracted much attention due to its non-degradability and bioaccumulation property [1,2]. Among those heavy metals, hexavalent chromium ions generated in the industry of electroplating, steel manufacturing, leather tanning, and textile production are a serious threat to the environment and human health [3,4].

* Corresponding authors.

The allowed maximum contaminant concentration regulated by the World Health Organization for total chromium in drinking water was 50 µg L^{-1} [5], hence, separation of Cr(VI) from wastewater is critical for the prevention of hexavalent chromium pollution in water.

Plentiful methods were applied to repair the waste water contaminated by hexavalent chromium, including ion exchange [6,7], membrane filtration [8,9], chemical reduction and precipitation [10], electrokinetic remediation [11,12], photocatalytic reduction [13–16], and adsorption [17–19]. Although ion exchange and membrane filtration techniques could separate dissolved heavy metal ions from water, a major shortage for its wide application was originated from its high operating costs [20]. Meanwhile, the main disadvantage of precipitation method is the generation of sludge [21]. Adsorption has been developed to be a cost-effective method to remove heavy metals, which has been widely studied in decades. However, adsorbents separation or recovery in heterogeneous systems remains a great challenge. Compared with the traditional adsorption separation methods, magnetic separation become attractive due to its benefits in separating pollutants and adsorbents from solution conveniently. For example, researchers reported that magnetite (Fe_3O_4) coated by humic acid could effectively remove Cr(VI) via adsorption and reduction pathway [22]. Meanwhile, magnetic manganese iron oxide also showed great prospect for environmental remediation [23–28]. Liu et al. [24] reported that magnetic zirconium-doped manganese ferrite could activate persulfate to generate hydroxyl radicals ($^{\bullet}OH$), sulfate radicals ($SO_4^{\bullet-}$), and superoxide radicals ($O_2^{\bullet-}$) for tetracycline degradation. Meanwhile, manganese ferrite dispersed over graphene sand could decompose methylene blue via photocatalytic mechanism [25]. Zhao et al. [26] applied nanocrystalline MFe_2O_4 (M = Mn, Fe, Co, Ni) materials to adsorb Congo red, and the magnetic separation could be achieved with high efficiency. Chen et al. [27] reported that magnetic manganese ferrite ($MnFe_2O_4$) nanoparticles treated by condensed air and NaOH solution could remove Cr(VI) in aqueous solution efficiently. Hamoudi et al. [28] reported that $MnFe_2O_4$ microspheres immobilized on the graphene nanosheets provided an attractive adsorbent for efficient glyphosate removal. Therefore, magnetic manganese ferrite materials exhibited promising performance for pollutants removal.

However, the magnetic properties resulted in the easy agglomeration property of its particles [29], which would decrease the activity of $MnFe_2O_4$ for pollutant removal. Considering that ultrasound is an effective technique for particles dispersion in aqueous solution via cavitation phenomenon [30], we intend to use ultrasound to obtain dispersed manganese ferrite. Meanwhile, the prepared $MnFe_2O_4$ may contain Mn(III) or Fe(II) in addition to Mn(II) and Fe(III) [31], and Mn(II) could be fully oxidized to Mn(IV) in a strong basic solution with oxygen added continuously (Eq. 1) [27]. The oxidized products of Mn(III)/Mn(IV) mineral could act as strong oxidants for the oxidation of Cr(III)-containing solids in turn. Moreover, the removal efficiency of Cr(VI) with zero-valent iron could be inhibited by 3 times in the presence of oxygen [32]. Therefore, it was speculated that the ubiquitous dissolved oxygen

might affect the Cr(VI) removal performance of $MnFe_2O_4$ via affecting the valence of manganese element.

$$2MnFe_2O_4 + 2NaOH + O_2 = 2MnO_2 + Fe_2O_3 + Na_2Fe_2O_4 + H_2O$$

(1)
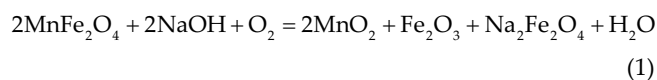
In this study, we prepared manganese ferrite via solvothermal method by mixing $MnCl_2 \cdot 4H_2O$ and $FeCl_3 \cdot 6H_2O$ in ethylene glycol solution with the addition of NaAc and polyethylene glycol. And then, we compared the performance of Cr(VI) removal in the absence or presence of dissolved oxygen with or without ultrasound pretreatment. Meanwhile, the morphology and composition of manganese ferrite before and after reaction were compared to illustrate the mechanism for Cr(VI) removal. This research aimed to provide fundamental theory for the wide application of magnetic manganese ferrite for water treatment.

2. Materials and methods

2.1. Chemicals

In this study, ferric chloride hexahydrate ($FeCl_3 \cdot 6H_2O$), manganese chloride tetrachloride ($MnCl_2 \cdot 4H_2O$), polyethylene glycol 1000, sodium acetate (NaAc), ethylene glycol, and potassium dichromate ($K_2Cr_2O_7$) were purchased from Sinopharm Chemical Reagent Co., Ltd., (China). All reagents employed in this study were of analytical grade. The deoxygenated water was obtained through bubbling Ar gas (Ar ≥ 99.9%, Hubei Minghui Gas Company, China) into deionized water at least for 30 min.

2.2. Manganese ferrite preparation

Manganese ferrite were synthesized by dissolving 1.0 g of $MnCl_2 \cdot 4H_2O$ and 2.7 g of $FeCl_3 \cdot 6H_2O$ in 80 mL of ethylene glycol solution at 40°C. And then, 3.0 g of polyethylene glycol 1000, and 6.0 g of sodium acetate (NaAc) were added into the ethylene glycol solution. The solution was stirred magnetically about 10 min until these reagents were dissolved. Subsequently, the mixed solution was transferred into the 100 mL of hydrothermal reactor and reacted at 200°C for 8 h. After reaction, the reactor was cooled to room temperature, and the obtained black powders were separated by magnet, washed by deionized water and absolute ethanol. Subsequently, the black powders were dried in air dry oven at 60°C. The detail preparation information was summarized in Fig. 1. The obtained manganese ferrite powder was grinded by agate mortar before use.

2.3. Batch experiments of Cr(VI) removal

In a typical Cr(VI) removal experiment, 0.05 g of manganese ferrite was dispersed in 1 mL of distilled water via ultrasound pretreatment around 30 s. Then, the obtained manganese ferrite suspension was added into 100 mL round bottom three-neck flasks containing 50 mL 2 mg L^{-1} of Cr(VI) solution to start the removal experiment. All experiments were conducted in duplicate at room temperature (25°C) in anoxic and/or oxic atmosphere. In detail, Cr(VI)
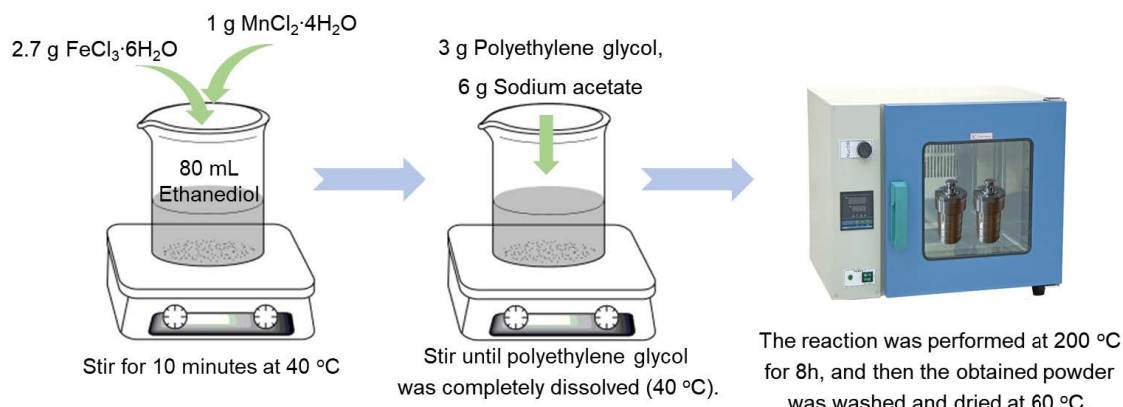
Fig. 1. Schematic diagram of manganese ferrite preparation procedure.

removal experiment under anoxic condition was conducted in deoxygenated water, the oxic experiments were carried out in deionized water open to air. During the removal experiment, 1 mL of sample solution was withdrawn at certain intervals and filtrated by 0.22 μm nylon filter. All the experiments were conducted three times.

For the cycling stability test of hexavalent chromium removal by manganese ferrite, we collected the particles after Cr(VI) adsorption reaction in air condition, and dried those powder in air dry oven at 60°C. And then, the collected manganese ferrite particles (0.05 g) were used to repeat the Cr(VI) adsorption experiment as we mentioned above. It was worth to note that more parallel Cr(VI) adsorption experiment by manganese ferrite should be conducted in the first cycle as the weight of manganese ferrite would loss during the recycle process.

2.4. Analytical method and characterization

Cr(VI) concentration in aqueous solution was analyzed by 1,5-diphenylcarbazide method with UV-vis spectrophotometer. Total iron ions and manganese ions concentration were monitored by atomic absorption spectrometry (200 Series AA, Agilent Technologies, USA). X-ray diffraction (XRD) patterns were obtained by Bruker D8 Advance X-ray diffractometer with Cu Kα radiation (λ = 1.54178 Å), and the voltage and current were set at 40 kV and 40 mA, respectively. Scanning electron microscopy (SEM) analysis was recorded on JSM-7100F (JEOL, Japan). X-ray photoelectron spectroscopy (XPS) was collected with ESCALAB 250 (Thermo Fisher, USA) and the binding energies were corrected by referencing the C 1s line at 284.8 eV.

3. Results and discussion

3.1. Manganese ferrite characterizations

The composite and morphology of the synthesized material were characterized with XRD, SEM and XPS. The XRD pattern revealed that diffraction peaks of pristine material with well crystalline structure could be ascribed to manganese iron oxide (JCPDF file No. 89-2807,

$Mn_{0.43}Fe_{2.57}O_4$), and the strong peak at 35.3° corresponding to the (311) crystal plane of manganese iron oxide (Fig. 2a). Further SEM images (Fig. 2b) shown that the morphology of manganese ferrite was of spherical shape in the diameter ranged from 50 to 200 nm. Due to the magnetic and electrostatic interactions, spherical particles of manganese ferrite would form clusters. Moreover, to investigate the chemical composition and valence state of the prepared manganese ferrite, XPS survey and high-resolution X-ray photoelectron spectroscopy (HR-XPS) of Mn 2p and Fe 2p were collected for further analysis. As shown in Fig. 3a, it could be observed that oxygen, manganese, and iron elements co-existed on the original manganese ferrite surface apart from the adventitious carbon with peak at 284.8 eV. Meanwhile, HR-XPS for Mn 2p shown that peaks located at 641.1 and 652.8 eV corresponding to Mn $2p_{1/2}$ and $2p_{3/2}$ (Fig. 3b), respectively, suggesting that presence of Mn^{2+} on the surface of manganese ferrite [33]. And the peak around 646.3 eV could be attributed to the satellite peak of Mn. For the Fe 2p spectrum, it could be found that peaks located at 710.4 and 724.0 eV were assigned to Fe^{3+} of $2p_{3/2}$ and Fe $2p_{1/2}$, respectively (Fig. 3c). Meanwhile, two peaks located at binding energies of around 718.5 and 732.5 eV could be attributed to the satellite peak of Fe^{3+} [34]. This result suggested the presence of Fe^{3+} on the surface of manganese ferrite.

3.2. Cr(VI) removal experiments

Subsequently, we further evaluated the Cr(VI) removal performance of the prepared manganese ferrite. As the magnetic property of manganese ferrite would result in particle aggregation, which would decrease the reactivity of manganese ferrite, ultrasound apparatus was used to make manganese ferrite dispersed. And then, we compared the Cr(VI) removal performance by manganese ferrite with or without ultrasound pretreatment. As shown in Fig. 4a, ultrasound pretreatment enhanced the Cr(VI) removal percentage with manganese ferrite from 33.6% to 100% within 120 min. It is well known that Cr(VI) could be removed through reduction and adsorption mechanism.
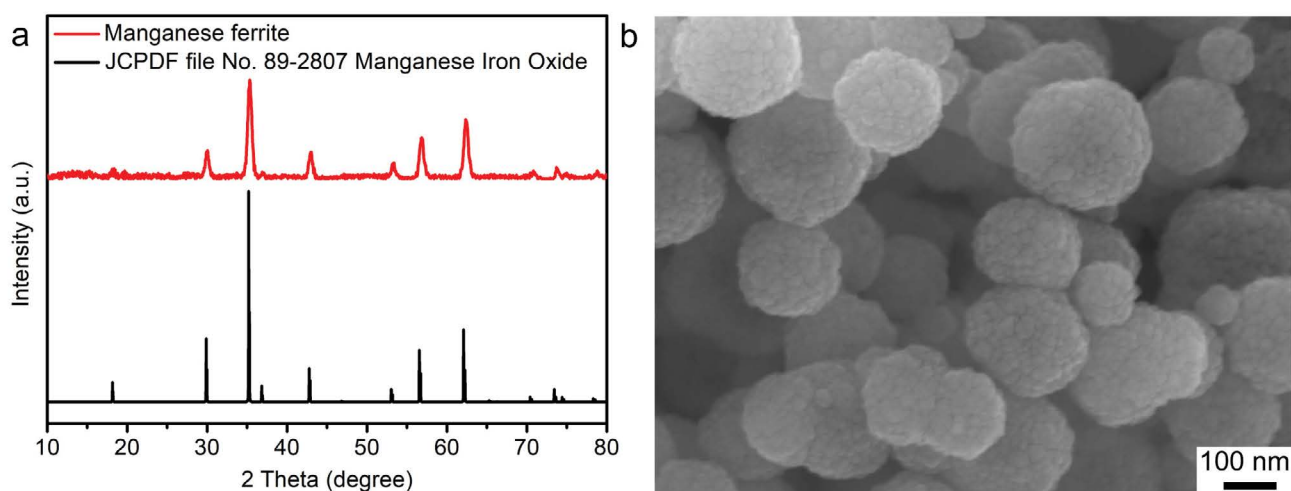
Fig. 2. (a) XRD pattern and (b) SEM image of pristine manganese ferrite.
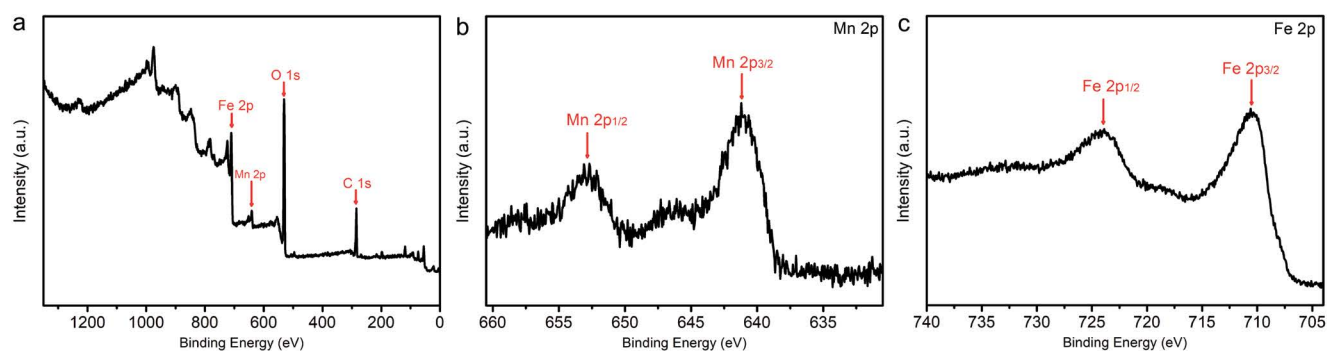

Fig. 3. Characterization of pristine manganese ferrite: (a) XPS survey, (b) HR-XPS spectrum of Mn 2p, and (c) HR-XPS spectrum of Fe 2p.

If reduction pathway was involved in the Cr(VI) removal process, the Cr(VI) removal efficiency in the aerobic atmosphere might be lower than that in the anoxic atmosphere as oxygen would compete with Cr(VI) for electron donated by manganese ferrite. Therefore, we further compared Cr(VI) removal efficiency in the aerobic or anoxic atmosphere. It was interesting to found that the absence of oxygen decreased the Cr(VI) removal percentage from 100% to 44.6% (Fig. 4a), suggesting that Cr(VI) was not removed through the reduction pathway. As pH value would affect the Cr(VI) removal performance, we therefore monitored the pH value variation during the Cr(VI) removal process. As shown in Fig. 4b, it was found that there were no significant differences between the pH values in the manganese ferrite/Air, manganese ferrite/US/Ar, and manganese ferrite/US/Air system, and all the pH value kept stable around 6 during the Cr(VI) removal process. Although Cr(VI) removal efficiency would be affected by pH value, the promoted Cr(VI) removal percentage in this study was not attributed to the pH value. To further investigate the reason for the promoted Cr(VI) removal in the presence of air, we further monitored the concentration variation of total manganese ions and iron ions. And the results elucidated that the presence of air enhanced the release of manganese ions and iron ions. As for the manganese ferrite/US/Air system, the concentration of total manganese ions increased to 1.28 mg L^{-1} in 20 min immediately, and then decreased to 0.85 mg L^{-1} at 120 min. Meanwhile, the total iron ions concentration increased to 0.15 mg L^{-1} within 120 min (Fig. 4c and d). In contrast, the maximum amount of released total manganese ion in the manganese ferrite/US/Ar and manganese ferrite/Air system at 20 min were only 1.08 and 0.63 mg L^{-1}, respectively, which was obviously lower than that in the manganese ferrite/US/Air system. Moreover, the dissolved iron ions concentration in the manganese ferrite/US/Ar and manganese ferrite/Air system were nearly not detectable with AAS, indicating that the enhanced Cr(VI) removal efficiency might be attributed to the flocculation and precipitation process of Cr(VI) by the promoted total manganese ions dissolution in the presence of dissolved oxygen. However, considering that manganese ions was regulated during water remediation, the released manganese ions should be treated further when manganese ferrite was applied in the practical application process.
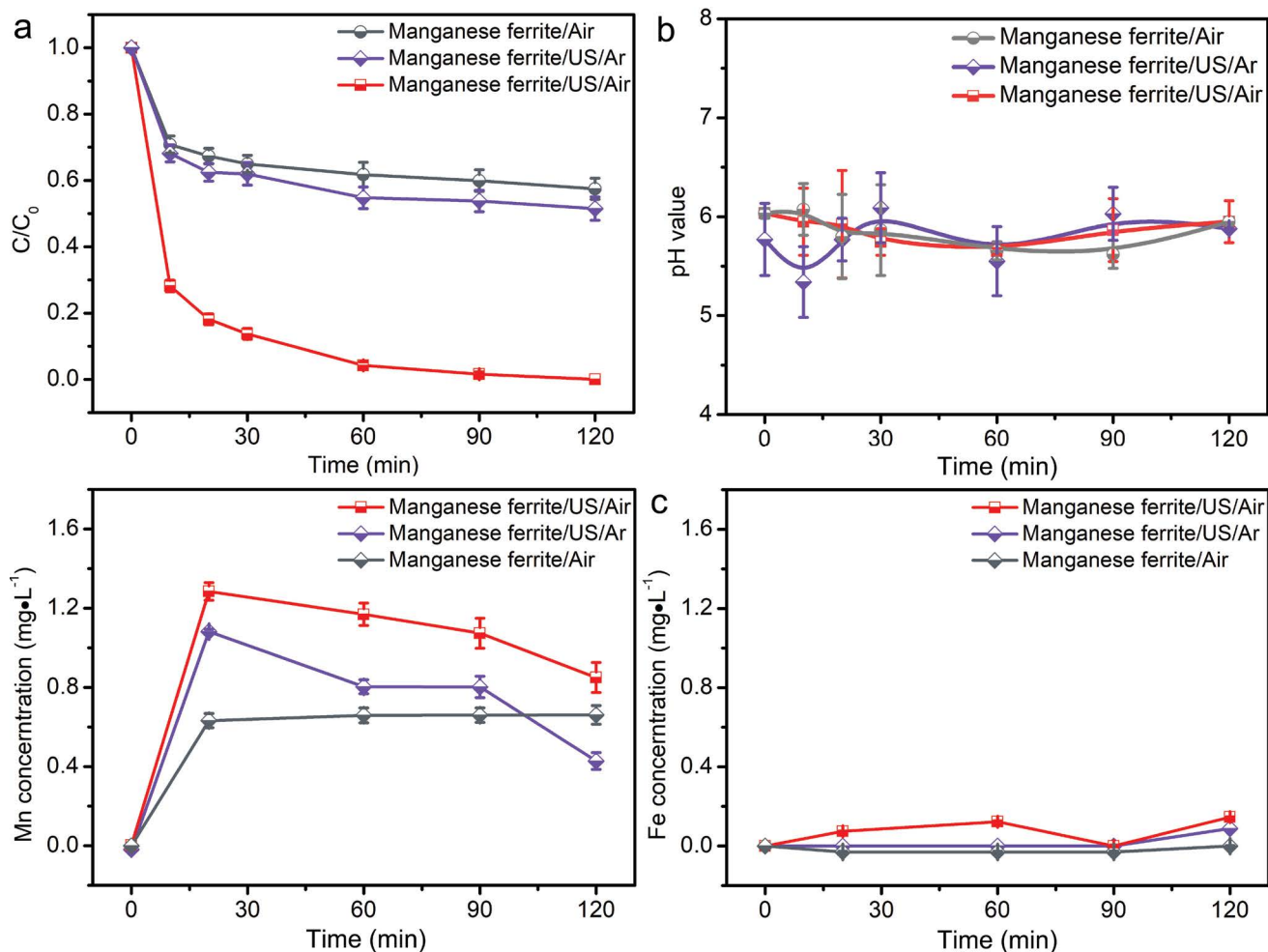
Fig. 4. (a) Cr(VI) removal by manganese ferrite with or without ultrasound pretreatment in the aerobic or anoxic atmosphere. (b) pH value variation during the Cr(VI) removal process with or without ultrasound pretreatment in the aerobic or anoxic atmosphere. (c) Concentration of total manganese ions vs. time determined by atomic absorption spectrum with or without ultrasound pretreatment in aerobic or anoxic atmosphere. (d) The concentration of total iron ions vs. time determined by atomic absorption spectrum with or without ultrasound pretreatment in aerobic or anoxic atmosphere. Reaction condition: [manganese ferrite]$_0$ = 0.05 g; [Cr(VI)]$_0$ = 2 mg L^{-1}. Error bars represent ± one standard deviation derived from triplicate experiments. Some standard deviations were smaller than symbols shown.

3.3. Mechanism of Cr(VI) removal with manganese ferrite

As the HR-XPS spectrum revealed that only Mn^{2+} existed on the surface of pristine manganese ferrite, and the reduction of Cr(VI) by Mn^{2+} was infeasible in theory [35–37]. Moreover, the oxidation of Mn^{2+} to Mn^{3+} would be accelerated by oxygen in air, and the dissolved Mn^{3+} could be disproportionated to generate manganese oxide (MnO$_X$) (Eq. 2) subsequently [38]. Hence, it was inferred that the generated nascent MnO$_X$ colloid provided more adsorption site for Cr(VI) removal in air condition than that in Ar condition.

$$Mn^{2+} + O_2 + H_2O \rightarrow MnO_X + H^+ \qquad (2)$$
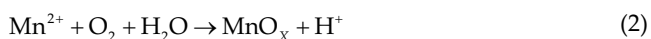
To verify this assumption, pyrophosphate, a kind of scavenger which could stabilize Mn^{3+} by avoiding Mn^{3+} be disproportionated [39], was added to the manganese ferrite/US/

Air system. The result suggested that 2 and 10 mmol L^{-1} of pyrophosphate could both totally inhibit the Cr(VI) removal (Fig. 5a). However, as the pyrophosphate was a kind of anion as well, which might compete the adsorption site with Cr(VI), and thus the inhibited effect might be attributed to the competitive adsorption process. Another kind of trapping agent for Mn^{3+}, n-hexanol, which could not be adsorbed on the surface of manganese ferrite, was therefore further used as trapping agent. As shown in Fig. 5b, there was no significant differences in the Cr(VI) removal efficiency with or without the addition of n-hexanol. Based on the Cr(VI) removal efficiency in the presence and absence of pyrophosphate and n-hexanol, it could be speculated that Cr(VI) was mainly removed through adsorption process, and the promoted Cr(VI) removal efficiency was not attributed to the precipitation by MnO$_X$ generated by the oxidation of Mn(II).
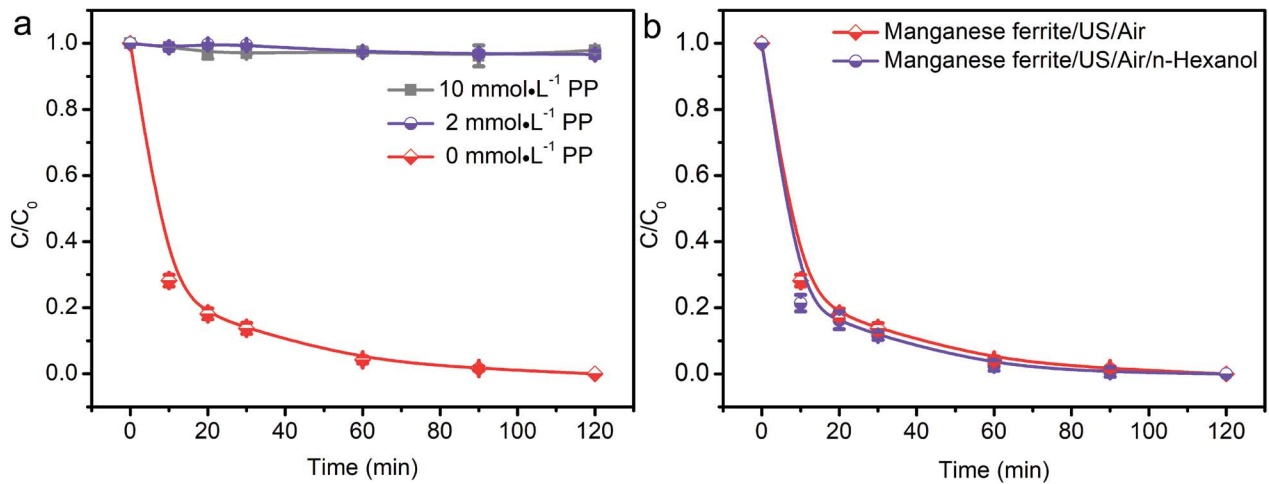
Fig. 5. (a) Removal curve of Cr(VI) with manganese ferrite in the presence and absence of pyrophosphate. (b) Cr(VI) removal by manganese ferrite with or without *n*-hexanol. Reaction condition: [manganese ferrite]$_0$ = 0.05 g; [Cr(VI)]$_0$ = 2 mg L^{-1}. Error bars represent ± one standard deviation derived from triplicate experiments. Some standard deviations were smaller than symbols shown.
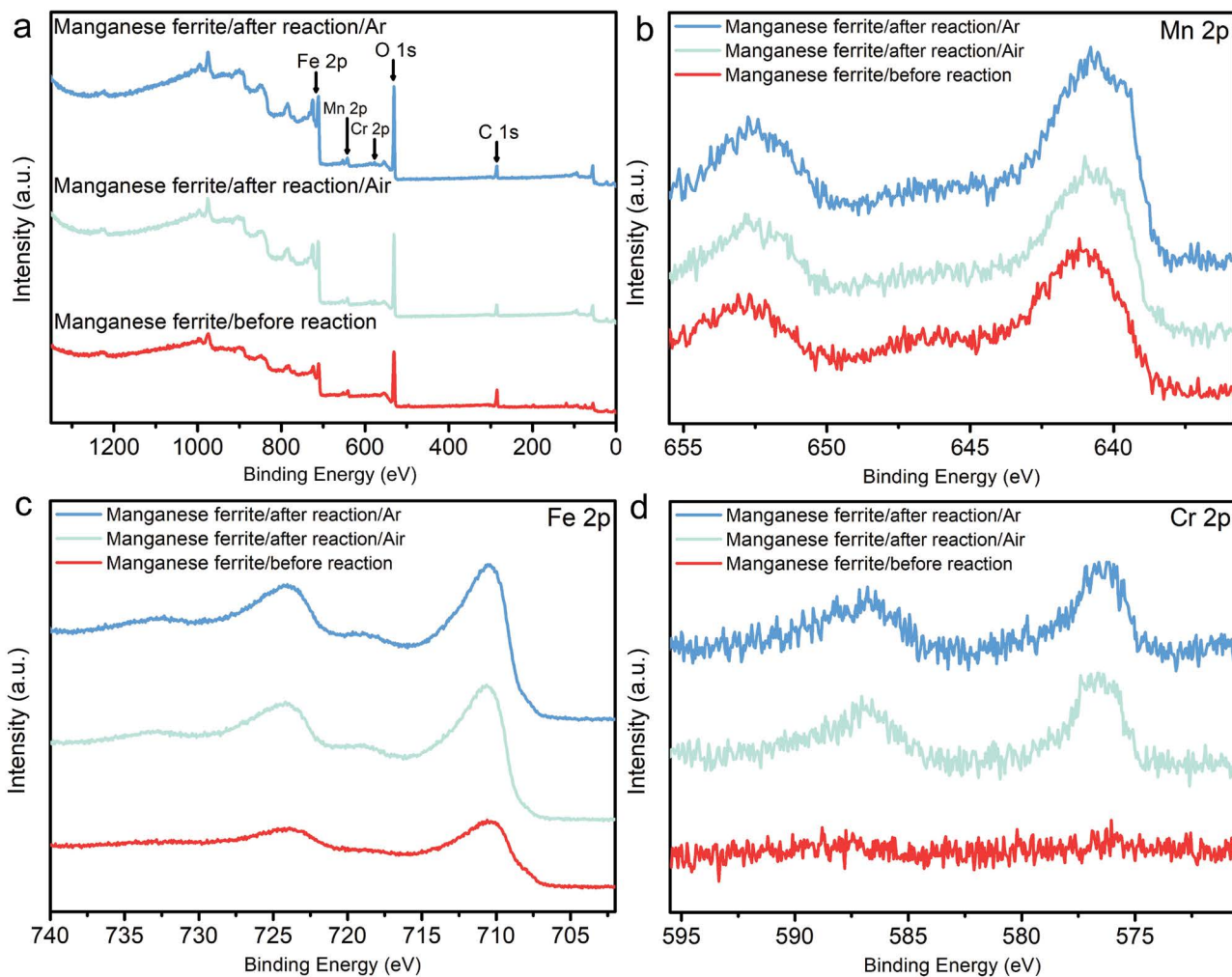

Fig. 6. HR-XPS spectra of manganese ferrite before and after the Cr(VI) removal in the presence of air and Ar: (a) Mn 2p, (b) Fe 2p and (c) Cr 2p.

In order to characterize the composition and valence variation of manganese ferrite before and after the Cr(VI) removal, we further compared the HR-XPS spectra of manganese ferrite for Mn 2p, Fe 2p, and Cr 2p. As shown in Fig. 6a, it could be found that peaks attributed to 2p3/2 and 2p1/2 of Cr(VI) around 578 eV appeared on the surface of manganese ferrite after the Cr(VI) removal experiment in air and Ar atmosphere [34], further confirming that Cr(VI) was removed via adsorption pathway. Meanwhile, there was no significant differences between the binding energies of HR-XPS spectra for Mn 2p and Fe 2p before and after Cr(VI) removal process (Fig. 6b and c), revealing that there was no valence variation in the Mn and Fe element of manganese ferrite.

To further confirm the adsorption mechanism, XRD was utilized to characterize the composition of manganese ferrite before and after the Cr(VI) removal. As shown in Fig. 7, no obvious differences could be found between manganese ferrite before and after Cr(VI) removal process in the presence of Ar and air. Based on the above characterization results, it could be concluded that Cr(VI) was removed through adsorption pathway, and no reduction process was involved.

3.4. Cyclic experiment

To evaluate the stability of the prepared manganese ferrite for Cr(VI) removal, we conducted the cycling experiment, and the result was exhibited in Fig. 8. It could be found that there was no significant difference between the first and the second Cr(VI) removal curve, while the third cycle result shown that the Cr(VI) removal percentage was only 87%, suggesting the decreased performance of manganese ferrite. Hence, further elution process was needed to obtain better Cr(VI) removal reactivity.

4. Conclusions

In this study, the influence of ultrasound pretreatment and dissolved oxygen on the Cr(VI) removal performance with magnetic manganese ferrite were investigated. Firstly, SEM, XRD, and XPS were applied to characterize the morphology and composition of the synthesized nanoparticles. The SEM results indicated that the prepared nanoparticles were spherical in the diameter ranged from 50 to 200 nm, and the XRD pattern matched well with manganese iron oxide. Further Cr(VI) removal experiments revealed that ultrasound pretreatment and dissolved oxygen enhanced the Cr(VI) removal percentage from 33.6% to 100% within 120 min. Although the dissolved manganese ion released under air atmosphere was obviously higher than that at Ar atmosphere, the enhanced Cr(VI) removal was not attributed to the precipitation by MnO_X generated by the oxidation of Mn(II). This study revealed the effect of ultrasound pretreatment and dissolved oxygen on the Cr(VI) removal efficiency and provided fundamental theory for the application of manganese ferrite for environmental remediation.
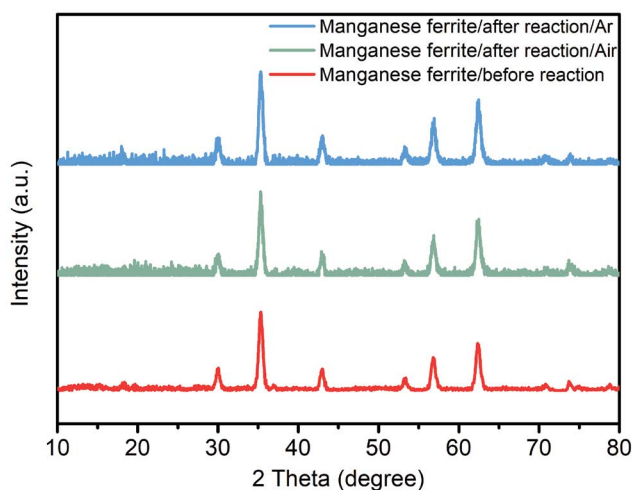

Fig. 7. XRD patterns of manganese ferrite before and after the Cr(VI) removal in the presence of air or Ar.

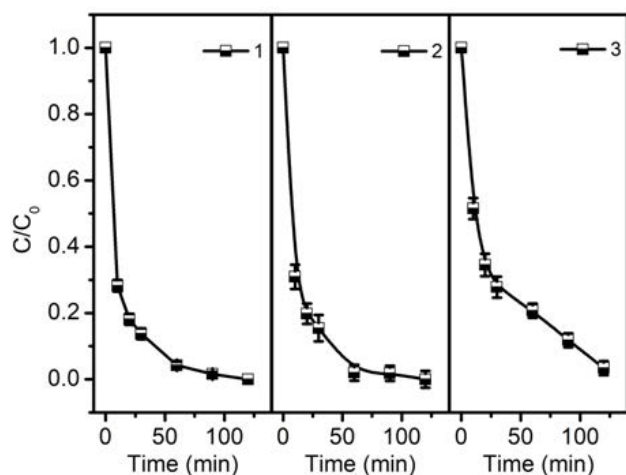

Fig. 8. Cycling stability test of hexavalent chromium removal by manganese ferrite. Reaction condition: [manganese ferrite]$_0$ = 0.05 g; [Cr(VI)]$_0$ = 2 mg L^{-1}. Error bars represent ± one standard deviation derived from triplicate experiments. Some standard deviations were smaller than symbols shown.

References

[1] P. Wijeyawardana, N. Nanayakkara, C. Gunasekara, A. Karunarathna, D. Law, B.K. Pramanik, Improvement of heavy metal removal from urban runoff using modified pervious concrete, Sci. Total Environ., 815 (2022) 152936, doi: 10.1016/j.scitotenv.2022.152936.
[2] J.F. Chin, Z.W. Heng, H.C. Teoh, W.C. Chong, Y.L. Pang, Recent development of magnetic biochar crosslinked chitosan on heavy

metal removal from wastewater – modification, application and mechanism, Chemosphere, 291 (2021) 133035, doi: 10.1016/j. chemosphere.2021.133035.

[3] S.A. Rosli, N. Alias, N. Bashirom, S. Ismail, W.K. Tan, G. Kawamura, A. Matsuda, Z. Lockman, Hexavalent chromium removal via photoreduction by sunlight on titanium–dioxide nanotubes formed by anodization with a fluorinated glycerol–water electrolyte, Catalysts, 11 (2021) 376, doi: 10.3390/catal11030376.

[4] F. Budiman, W.K. Tan, G. Kawamura, H. Muto, A. Matsuda, K. Abdul Razak, Z. Lockman, Formation of dense and high-aspect-ratio iron oxide nanowires by water vapor-assisted thermal oxidation and their Cr(VI) adsorption properties, ACS Omega, 6 (2021) 28203–28214.

[5] Z. Pan, X. Zhu, A. Satpathy, W. Li, J.D. Fortner, D.E. Giammar, Cr(VI) adsorption on engineered iron oxide nanoparticles: exploring complexation processes and water chemistry, Environ. Sci. Technol., 53 (2019) 11913–11921.

[6] J.A. Korak, R. Huggins, M. Arias-Paic, Regeneration of pilot-scale ion exchange columns for hexavalent chromium removal, Water Res., 118 (2017) 141–151.

[7] H. Wang, X. Song, H. Zhang, P. Tan, F. Kong, Removal of hexavalent chromium in dual-chamber microbial fuel cells separated by different ion exchange membranes, J. Hazard. Mater., 384 (2020) 121459, doi: 10.1016/j.jhazmat.2019.121459

[8] A. Bratovcic, H. Buksek, C. Helix-Nielsen, I. Petrinic, Concentrating hexavalent chromium electroplating wastewater for recovery and reuse by forward osmosis using underground brine as draw solution, Chem. Eng. J., 431 (2022) 133918, doi: 10.1016/j.cej.2021.133918.

[9] N. Dizge, Y. Ozay, M. Boussemghoune, M. Chikhi, Preparation of catalytic polyether sulfone coated ceramic membrane for reduction of hexavalent chromium, J. Water Process Eng., 40 (2021) 101946, doi: 10.1016/j.jwpe.2021.101946.

[10] W. Shen, J. Zhang, M. Xiao, X. Zhang, J. Li, W. Jiang, J. Yan, Z. Qin, S. Zhang, W. He, Y. He, Ethylenediaminetetraacetic acid induces surface erosion of zero-valent iron for enhanced hexavalent chromium removal, Appl. Surf. Sci., 525 (2020) 146593, doi: 10.1016/j.apsusc.2020.146593.

[11] H. Xu, J. Bai, X. Yang, C. Zhang, M. Yao, Y. Zhao, Lab scale-study on the efficiency and distribution of energy consumption in chromium contaminated aquifer electrokinetic remediation, Environ. Technol. Innovation, 25 (2022) 102194, doi: 10.1016/j. eti.2021.102194.

[12] X. He, G. Cui, Q. Zhang, Z. Wang, T. Tang, Y. Liu, Application of sulfide-modified nanoscale zerovalent iron electrodes for electrokinetic remediation of chromium-contaminated soil in a three-dimensional electrode system, J. Environ. Chem. Eng., 9 (2021) 106791, doi: 10.1016/j.jece.2021.106791.

[13] N. Luo, C. Chen, D. Yang, W. Hu, F. Dong, S defect-rich ultrathin 2D MoS$_2$: the role of S point-defects and S stripping-defects in the removal of Cr(VI) via synergistic adsorption and photocatalysis, Appl. Catal., B, 299 (2021) 120664, doi: 10.1016/j. apcatb.2021.120664.

[14] Z. Jiang, K. Chen, Y. Zhang, Y. Wang, F. Wang, G. Zhang, D.D. Dionysiou, Magnetically recoverable MgFe$_2$O$_4$/conjugated polyvinyl chloride derivative nanocomposite with higher visible-light photocatalytic activity for treating Cr(VI)-polluted water, Sep. Purif. Technol., 236 (2020) 116272, doi: 10.1016/j. seppur.2019.116272.

[15] T. Ge, Z. Jiang, L. Shen, J. Li, Z. Lu, Y. Zhang, F. Wang, Synthesis and application of Fe$_3$O$_4$/FeWO$_4$ composite as an efficient and magnetically recoverable visible light-driven photocatalyst for the reduction of Cr(VI), Sep. Purif. Technol., 263 (2021) 118401, doi: 10.1016/j.seppur.2021.118401.

[16] Q. Zhao, X.-H. Yi, C.-C. Wang, P. Wang, W. Zheng, Photocatalytic Cr(VI) reduction over MIL-101(Fe)–NH$_2$ immobilized on alumina substrate: from batch test to continuous operation, Chem. Eng. J., 429 (2022) 132497, doi: 10.1016/j.cej.2021.132497.

[17] V.M. Boddu, K. Abburi, J.L. Talbott, E.D. Smith, Removal of hexavalent chromium from wastewater using a new composite chitosan biosorbent, Environ. Sci. Technol., 37 (2003) 4449–4456.

[18] T. Kekes, G. Kolliopoulos, C. Tzia, Hexavalent chromium adsorption onto crosslinked chitosan and chitosan/β-cyclodextrin beads: novel materials for water decontamination, J. Environ. Chem. Eng., 9 (2021) 105581, doi: 10.1016/j.jece.2021.105581.

[19] S. Mortazavian, H. An, D. Chun, J. Moon, Activated carbon impregnated by zero-valent iron nanoparticles (AC/nZVI) optimized for simultaneous adsorption and reduction of aqueous hexavalent chromium: material characterizations and kinetic studies, Chem. Eng. J., 353 (2018) 781–795.

[20] S. Shahrin, W.-J. Lau, P.-S. Goh, J. Jaafar, A.F. Ismail, Adsorptive removal of As(V) ions from water using graphene oxide-manganese ferrite and titania nanotube-manganese ferrite hybrid nanomaterials, Chem. Eng. Technol., 41 (2018) 2250–2258.

[21] G. Qin, M.J. McGuire, N.K. Blute, C. Seidel, L. Fong, Hexavalent chromium removal by reduction with ferrous sulfate, coagulation, and filtration: a pilot-scale study, Environ. Sci. Technol., 39 (2005) 6321–6327.

[22] W. Jiang, Q. Cai, W. Xu, M. Yang, Y. Cai, D.D. Dionysiou, K.E. O'Shea, Cr(VI) adsorption and reduction by humic acid coated on magnetite, Environ. Sci. Technol., 48 (2014) 8078–8085.

[23] H. Yi, C. Lai, X. Huo, L. Qin, Y. Fu, S. Liu, L. Li, M. Zhang, M. Chen, G. Zeng, H$_2$O$_2$-free photo-Fenton system for antibiotics degradation in water via the synergism of oxygen-enriched graphitic carbon nitride polymer and nano manganese ferrite, Environ. Sci.: Nano, 9 (2022) 815–826.

[24] Z. Liu, Z. Gao, Q. Wu, Activation of persulfate by magnetic zirconium-doped manganese ferrite for efficient degradation of tetracycline, Chem. Eng. J., 423 (2021) 130283, doi: 10.1016/j. cej.2021.130283.

[25] A.J.R. Luciano, L. de Sousa Soletti, M.E.C. Ferreira, L.F. Cusioli, M.B. de Andrade, R. Bergamasco, N.U. Yamaguchi, Manganese ferrite dispersed over graphene sand composite for methylene blue photocatalytic degradation, J. Environ. Chem. Eng., 8 (2020) 104191, doi: 10.1016/j.jece.2020.104191.

[26] L. Wang, J. Li, Y. Wang, L. Zhao, Q. Jiang, Adsorption capability for Congo red on nanocrystalline MFe$_2$O$_4$ (M = Mn, Fe, Co, Ni) spinel ferrites, Chem. Eng. J., 181–182 (2012) 72–79.

[27] J. Hu, Lo, G. Chen, Fast removal and recovery of Cr(VI) using surface-modified jacobsite (MnFe$_2$O$_4$) nanoparticles, Langmuir, 21 (2005) 11173–11179.

[28] N. Ueda Yamaguchi, R. Bergamasco, S. Hamoudi, Magnetic MnFe$_2$O$_4$–graphene hybrid composite for efficient removal of glyphosate from water, Chem. Eng. J., 295 (2016) 391–402.

[29] T. Wang, L. Zhang, H. Wang, W. Yang, Y. Fu, W. Zhou, W. Yu, K. Xiang, Z. Su, S. Dai, L. Chai, Controllable synthesis of hierarchical porous Fe$_3$O$_4$ particles mediated by poly(diallyldimethylammonium chloride) and their application in arsenic removal, ACS Appl. Mater. Interfaces, 5 (2013) 12449–12459.

[30] Y.-C. Chen, P. Smirniotis, Enhancement of photocatalytic degradation of phenol and chlorophenols by ultrasound, Ind. Eng. Chem. Res., 41 (2002) 5958–5965.

[31] G. Bonsdorf, K. Schäfer, K. Teske, H. Langbein, H. Ullmann, Stability region and oxygen stoichiometry of manganese ferrite, Solid State Ionics, 110 (1998) 73–82.

[32] Y. Mu, H. Wu, Z. Ai, Negative impact of oxygen molecular activation on Cr(VI) removal with core-shell Fe@Fe$_2$O$_3$ nanowires, J. Hazard. Mater., 298 (2015) 1–10.

[33] Y. Fu, P. Xiong, H. Chen, X. Sun, X. Wang, High photocatalytic activity of magnetically separable manganese ferrite–graphene heteroarchitectures, Ind. Eng. Chem. Res., 51 (2012) 725–731.

[34] J.F. Moulder, W.F. Stickle, P.E. Sobol, K.D. Bomben, Handbook of X-ray Photoelectron Spectroscopy: A Reference Book of Standard Spectra for Identification and Interpretation of XPS Data, Perkin-Elmer Corporation Physical Electronics Division, United States of America, 1992.

[35] C.F. Huber, G.P. Haight, The oxidation of manganese(II) by chromium(VI) in the presence of oxalate ion, J. Am. Chem. Soc., 98 (1976) 4128–4131.

[36] K.U. Din, K. Hartani, Z. Khan, Effect of micelles on the oxidation of oxalic acid by chromium(VI) in the presence and absence of manganese(II), Colloids Surf., A, 193 (2001) 1–13.

[37] B. Sarkar, R. Naidu, G.S.R. Krishnamurti, M. Megharaj, Manganese(II)-catalyzed and clay-minerals-mediated reduction of chromium(VI) by citrate, Environ. Sci. Technol., 47 (2013) 13629–13636.

[38] W. Liu, J. Li, J. Zheng, Y. Song, Z. Shi, Z. Lin, L. Chai, Different pathways for Cr(III) oxidation: implications for Cr(VI) reoccurrence in reduced chromite ore processing residue, Environ. Sci. Technol., 54 (2020) 11971–11979.

[39] W. Liu, B. Sun, J. Qiao, X. Guan, Influence of pyrophosphate on the generation of soluble Mn(III) from reactions involving Mn oxides and Mn(VII), Environ. Sci. Technol., 53 (2019) 10227–10235.